Proceedings of the 4th International Conference on Environmental Pollution and Remediation
Prague, Czech Republic, August 11-13, 2014
Paper No. 81

Guidelines for Preliminary Design of Funnel-and-gate Reactive Barriers

Benoît Courcelles
Polytechnique Montréal, Department of Civil, Geological and Mining Engineering
CP 6079, Succ. Centre-Ville, Montréal, Qc, H3C 3A7, Canada
benoit.courcelles@polymtl.ca

Abstract **-** Permeable Reactive Barriers represent an innovative remediation technique of contaminated aquifers. Three geometric configurations are encountered in the literature: a continuous wall, a funnel-and-gate system, and a caisson configuration. The present paper is focused on the design of the second and third geometric configurations and presents an analytical solution of the flow in a Permeable Reactive Barrier based on the Schwarz-Christoffel transformation. This analytical solution is coupled to residence time calculations to define a methodology of design taking into account the most important parameters on the design of a PRB: cut-off width, slenderness of the reactive cell, and hydraulic conductivity. Finally, the study provides a guidance diagram for the design of funnel-and-gate or caisson configurations.

Keywords**:** Permeable Reactive Barrier, Contamination, Groundwater, Analytical study, Design.

1. Introduction

Permeable reactive barriers (PRBs) constitute a passive remediation technique for the treatment of polluted groundwater (Blowes, Ptacek et al. 1995). Their principle relies on the exploitation of hydraulic gradients to treat the groundwater in a reactive media able to degrade, adsorb or precipitate the pollutants.

Three main geometric configurations are available in the literature: (a) a continuous wall (CW) composed of reactive trenches or injection wells (Blowes, Ptacek et al. 1995); (b) a funnel-and-gate configuration (F&G) composed of two impermeable walls that direct the contaminated plume towards a filtering gate (McMurtry and Elton 1985); and (c) a caisson configuration (CC) similar to the previous one, but in which the flow in the filtering gate is in the upward direction (Warner, Yamane et al. 1998).

As regards the implementation of each configuration, continuous walls represent the common type of PRB (Blowes, Ptacek et al. 1995). A design methodology is dedicated to this configuration and relies on the residence time of pollutants in the reactive media (Powell, Blowes et al. 1998; Gavaskar 1999). On the contrary, only few practical tools are available in the literature for the design of funnel-and-gate PRBs and they are particularly focused on the hydraulic behaviour of PRBs (Klammler and Hatfield 2009; Klammler, Hatfield et al. 2010; Klammler, Hatfield et al. 2010). However, the design of such PRBs relies on three technical aspects: (a) the reactive media must be appropriate to the pollutants, (b) the filters' size must be large enough to ensure a sufficient residence time (Shoemaker, Greiner et al. 1995; Warren, Arnold et al. 1995; O'Hannesin and Gillham 1998), and (c) the reactive material must have a sufficient hydraulic conductivity to prevent any bypass of the system (Painter 2004).

Hydrologic characteristics of groundwater flows represent a challenge for the design of PRBs (Liu, Li et al. 2011). Assuming that the reactive material is adequately selected from laboratory tests, the two interdependent parameters for the design of PRBs are the residence time and the hydraulic capture width. Residence time refers to the contact time between the contaminated groundwater and the reactive media within the barrier. It ensures that the reactive barrier is large enough to meet regulatory requirements. Hydraulic capture width refers to the maximal width of the contaminated groundwater that can enter a filtering gate or go through a continuous wall.

Numerical modeling constitutes the most popular option for the design of PRBs and commercial software products such as MODFLOW (McDonald and Harbaugh 1988) and FLONET (Guiger, Molson et al. 1991) are extensively used to evaluate the effect of PRBs on regional flows. Nevertheless, this approach is cost and time consuming. To face this problem, several authors have considered an analytic approach for preliminary design and optimization of PRBs. Thus, Craig and al. (2006) chose the Analytic Element Method (AEM) to represent a continuous wall in a homogenous aquifer. Their model was based on an elliptical inhomogeneity placed in a uniform flow as a representation of a PRB. This approach constituted a first step in analytical modeling and provided useful tools for preliminary designs. To expand on the approximation of an elliptic geometry, Klammler and Hatfield (2008) investigated another approach based on conformal mapping and obtained solutions for flow fields around a rectangular continuous wall. This approach has been later extended to funnel-and-gate and drain-and-gate configurations (Klammler and Hatfield 2009; Klammler, Hatfield et al. 2010) and the authors analysed the solutions for flow fields regarding widths and shapes of the capture zones under different scenarios. These anterior works are particularly useful for preliminary design of F&G, but they are mainly focused on hydraulic aspects of the design. As the residence time in reactive filters is an essential element, the originality of the present paper consists in considering the residence time as an additional criterion for preliminary design of permeable reactive barriers.

2. Schwarz-Christoffel Theorem

The Schwarz-Christoffel theorem states that the interior of a closed polygon may be mapped into the upper half of a plane (Streeter 1948). This transformation is illustrated in Fig. 1.a and b, where the function *f* transforms the real axis in the z-diagram into a polygon in the z'-diagram. The inverse transformation is represented by the function *g*. Eq. 1 represents the Schwarz-Christoffel transformation.

A

$$\frac{dz\prime}{dz} = \frac{d}{dz}[f(z)] = \frac{\gamma}{(x_A - z)^{\alpha_1/\pi} \cdot (x_B - z)^{\alpha_2/\pi} \cdot (x_C - z)^{\alpha_3/\pi} \cdot (x_D - z)^{\alpha_4/\pi} \ldots} \quad (1)$$

where γ is a complex number in the z-diagram; *f* is a complex function; x_A, x_B, x_C, x_D,… are real constants in ascending order of magnitude; α_1, α_2, α_3, α_4, … are external angles of the polygon. Considering $\alpha_1 = \pi/2$; $\alpha_2 = -\pi$ and $\alpha_3 = \pi/2$, Eq. 1 becomes Eq. 2 and transforms the real axis (Fig. 1.c) into a polygon with two apexes at infinity (Fig. 1.d). In particular, this transformation states that a flow around a cut-off wall perpendicular to a uniform flow can be deduced from a uniform flow without any PRB. Indeed, the x-axis can be considered as a no-flow boundary condition for a uniform flow parallel to this axis in the z-diagram (Fig. 1.c). In the z'-diagram (Fig. 1.d), this no-flow boundary is transformed into the negative part of the x'-axis, two segments [AB] and [BC] along the y'-axis, and the positive part of the x'-axis. Considering [AB] and [BC] as the upstream and downstream sides of an half cut-off wall, the basic set of boundary conditions in the z-diagram is mapped over a more complex geometry in the z'-diagram. As the flow in the lower half of the z'-diagram (respectively z-diagram) can be deduced from the flow in the upper half by symmetry, the analytical solution will be established for $Y>0$ (respectively $y>0$).

$$\frac{dz\prime}{dz} = \frac{d}{dz}[f(z)] = \frac{\gamma \cdot z}{\sqrt{z^2 - R^2}} \quad (2)$$

where *R* is a real positive number equal to the half-length of the cut-off wall. After integration (Eq. 3) and introduction of two set of images, $f(z=0) = iR$ and $f(z=R) = 0$, the analytical expressions of the function *f* and its inverse function *g* are respectively given in Eq. 4 and Eq. 5.

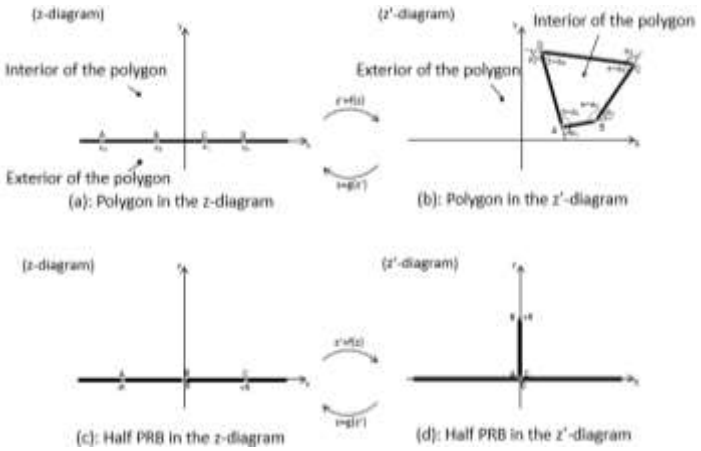

Fig. 1. Schwarz-Christoffel's principle.

$$z' = f(z) = \gamma \int \frac{z}{\sqrt{z^2 - R^2}} \cdot dz + B \tag{3}$$

$$z' = f(z) = \sqrt{z^2 - R^2} \tag{4}$$

$$z = g(z') = \sqrt{z'^2 + R^2} \tag{5}$$

Introducing the real and imaginary part of complex numbers $z = x+iy$ and $z' = X+iY$, Eq. 5 can be rewritten as:

$$(x + iy)^2 = (X + iY)^2 + R^2 \tag{6}$$

Development and separation of the real and imaginary parts leads to the following system of equations where the origins in the z and z'-diagrams are not considered in the domain (apex of the polygon in the z'-diagram):

$$\begin{cases} x^2 - y^2 = X^2 - Y^2 + R^2 \\ xy = XY \end{cases} \tag{7}$$

This system of equations is easily solved and leads to a fourth order polynomial whose roots are given in Eq. 8. Considering that y is strictly positive in the upper half of the z-diagram, the expression of y is given in Eq. 9.

$$x = \delta_X \cdot \sqrt{\frac{X^2 - Y^2 + R^2 + \sqrt{(X^2 - Y^2 + R^2)^2 + 4X^2Y^2}}{2}} \tag{8}$$

$$y = \delta_X \cdot \frac{XY}{\sqrt{\frac{X^2 - Y^2 + R^2 + \sqrt{(X^2 - Y^2 + R^2)^2 + 4X^2Y^2}}{2}}} \tag{9}$$

where δ_X represent the sign of X. The previous equations are particularly interesting because they represent a flow around a cut-off wall. In the next section, the geometry will be complicated by permitting

a flow across the cut-off wall at the origin. This additional boundary condition represents the filtering gate (reactor).

2.1 Complex Potential Ω around a PRB

In the present model, the widths of the cut-off wall and the reactive zone are neglected in comparison to the dimensions of the regional groundwater flow. Moreover, the filtering gate is represented by a sink and a source located respectively upstream and downstream of the cut-off wall. This assumption is particularly interesting to represent the flow in the z'-diagram as a function of a simple geometry in the z-diagram. Indeed, if we consider a sink located at point *A* and another at point *C* in the z-diagram (see Fig. 1.c), the image in the z'-diagram becomes a funnel-and-gate PRB.

Considering a steady, uniform and irrotational flow in the z-diagram, Eq. 10 represents the velocity potential ϕ and the stream function ψ.

$$\begin{cases} \phi = -V_0 \cdot x \\ \psi = -V_0 \cdot y \end{cases} \tag{10}$$

where V_0 is a constant velocity parallel to the x-axis in the z-diagram. Considering a sink and a source of equal strength q respectively located at *(-R,0)* and *(+R,0)* in an initially static aquifer, the velocity potential ϕ and the stream function ψ are given in Eq. 11 (Chanson 2009).

$$\begin{cases} \phi = -\frac{q}{4\pi} \cdot ln\left(\frac{(x-R)^2+y^2}{(x+R)^2+y^2}\right) \\ \psi = -\frac{q}{2\pi} \cdot \left(tan^{-1}\left(\frac{y}{x-R}\right) - tan^{-1}\left(\frac{y}{x+R}\right)\right) \end{cases} \tag{11}$$

where q is the flow rate per meter of depth of the aquifer (m^2/s). According to the superposition principle, the addition of Eq. 10 and Eq. 11 gives the velocity potential and the stream function of a uniform flow influenced by a sink and a source. Replacing *x* and *y* by Eq. 8 and 9, we obtain the velocity potential and stream function around a PRB. This potential function has been introduced into Winplot-2d and the equipotential lines are illustrated on Fig. 2 for a cut-off wall of 160 m coupled with a sink and a source of 12 m^2/d. This figure also illustrates the capture zone and the by-pass of the PRB (groundwater laterally away from the x'-axis, outside of the envelope curve).

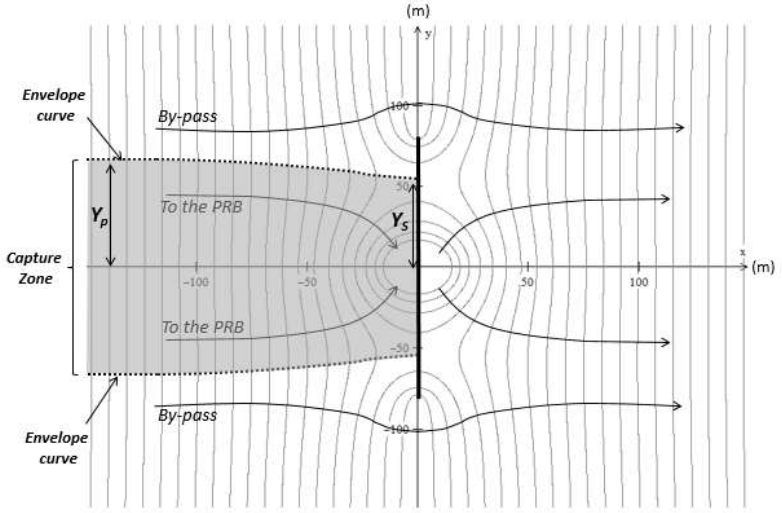

Fig. 2. Equipotential around a Permeable Reactive Barrier (bold) and sketch of flow lines (arrows).

As regards the hydraulic design of a PRB, the width of the plume caught by the filtering gate constitutes the most important information to be known. To determine this width, we studied the envelope

curve in the z-diagram and considered its transformation by the function *f*. Looking at the stagnation points in the z-diagram, three configurations can be observed depending on the magnitude of the flow rate q. These configurations are: (a) two stagnation points on the x-axis (Fig. 3a), (b) a stagnation point at the origin, or (c) two stagnation points on the y-axis (Fig. 3b). In the last case, some flow occurs from the source to the sink (recirculation). Considering that the sink and the source are connected through the filtering gate, this configuration cannot be encountered on the field and the water always goes from the sink to the source via the reactor. In the z-diagram, the abscissas of the two stagnation points (x_S in Fig. 3.a.) are given in Eq.12 and we can easily demonstrate that their images are located on the y'-axis of the z'-diagram. Their ordinates Y_S is given in Eq. 13. As Y_s cannot be higher than R (half-length of the cut-off wall), the maximum flow rate q that can enter the filtering gate is $\pi \cdot R \cdot V_0$.

$$x_S = \pm R \cdot \sqrt{1 - \frac{q}{\pi \cdot R \cdot V_0}} \tag{12}$$

$$Y_S = \pm\sqrt{R^2 - x_S^2} \tag{13}$$

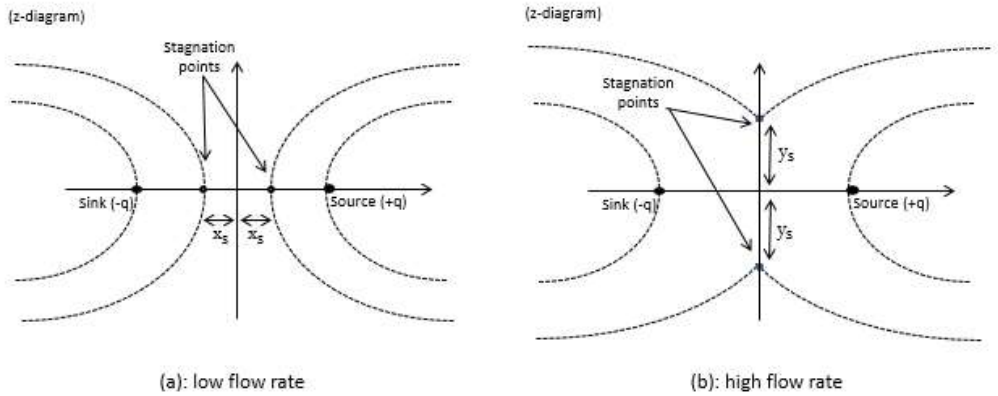

Fig. 3. Uniform flow past a sink and a source of equal strength.

Moreover, the formulation of the stream line towards the stagnation point in the z-diagram is given in Eq. 14 (Chanson 2009).

$$\psi_0 = -\frac{q}{2\pi} \cdot \left(tan^{-1}\left(\frac{y}{x-R}\right) - tan^{-1}\left(\frac{y}{x+R}\right)\right) - V_0 \cdot y = -\frac{q}{2} \tag{14}$$

Considering the limit of the stream function when $x \to -\infty$ ($or\ X \to -\infty$), we obtain the half-width of the capture zone entering the reactor (see Eq. 15 and Y_p in Fig. 4.b.).

$$Y_p = y_p = -\frac{\psi_0}{V_0} \tag{15}$$

Combining Eq.14 and 15, we can demonstrate that the half width of the capture zone is proportional to q and inversely proportional to the initial velocity of the flow V_0 (see Eq. 16).

$$Y_p = \frac{q}{2 \cdot V_0} \tag{16}$$

To illustrate the displacement of the envelope curve as a function of the flow rate q, different values of q from 0.1 to 1 m^2/h are introduced in Eq. 14 and the solutions are provided on Fig. 4. For every single $x \in]-\infty; x_S]$, the corresponding ordinate y is calculated thanks to the Generalized Reduced Gradient method (GRG) due to the non-linearity of Eq. 14. The image of the envelope curve has then been calculated in the z'-diagram. The capture width Y_p is smaller than the ordinate Y_s of the stagnation point for small flow rates, whereas Y_p is greater than Y_s for high flow rates. Nevertheless, this illustration cannot yet be considered as a real flow net around a PRB as the flow rate in the reactor q is not a boundary condition, but is imposed by the geometry of the reactor and its related hydraulic head losses. As a consequence, the model is extended in the next section by considering the geometry of the reactor and its impact on the flow rate.

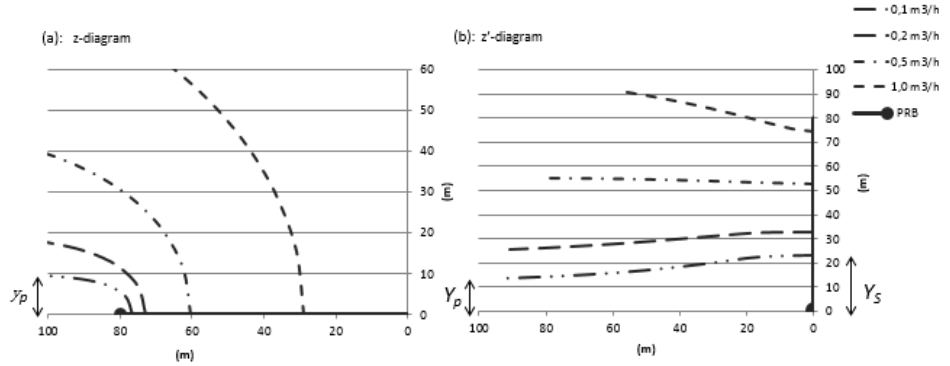

Fig. 4. envelope curves in the z and z'-diagrams.

2.2 Flow Rate in a Filtering Gate

The previous representation of the filtering gate means that the velocity potentials are respectively set to -∞ and +∞ at the sink and the source. This assumption represents a bias because the velocity potential must be a continuous function across the reactor and the values at the entrance and the exit must be finite. To be more realistic, we considered the radius r_w of two wells representing the sink and the source in the z-diagram. Thus, the velocity potentials upstream (ϕ_u^w) and downstream (ϕ_d^w) related to these two wells are defined in Eq. 17 and 18 and their difference is given in Eq. 19.

$$\phi_u^w = -\frac{q}{4\pi} \cdot ln\left(\frac{(2R+r_w)^2}{r_w^2}\right) \tag{17}$$

$$\phi_d^w = -\frac{q}{4\pi} \cdot ln\left(\frac{r_w^2}{(2R+r_w)^2}\right) \tag{18}$$

$$\phi_d^w - \phi_u^w = -\frac{q}{\pi} \cdot ln\left(\frac{r_w}{2R+r_w}\right) \tag{19}$$

This difference is combined to $\phi_d^v - \phi_u^v$ (velocity potential induced by a uniform velocity field in the z-diagram) to obtain the overall velocity field presented in Eq. 21.

$$\phi_d^v - \phi_u^v = -2 \cdot V_0 \cdot R \tag{20}$$

$$\phi_d - \phi_u = \phi_d^v - \phi_u^v + \phi_d^w - \phi_u^w = -2 \cdot V_0 \cdot R - \frac{q}{\pi} \cdot ln\left(\frac{r_w}{2R+r_w}\right) \tag{21}$$

As r_w represents the radius of the gravel pack around the wells in the z-diagram, we can easily demonstrate that the image of the gravel pack around the sink (respectively the source) is a half-gravel pack located upstream (respectively downstream) of the cut-off wall in the z'-diagram. The radius of gravel packs in the z'-diagram (R_d) can be deduced from the function g (see Eq. 22).

$$R_d = \sqrt{(r_w + R)^2 - R^2} \tag{22}$$

$$r_w = -R + \sqrt{R^2 + R_d^2} \tag{23}$$

Otherwise, Darcy's law in a reactive filter states that the flow rate Q entering a filtering gate is proportional to its hydraulic conductivity, its surface and the hydraulic gradient. Considering that the head losses are generated by the porous media and negligible for all pipes or draining trenches that can be implemented at the entrance and the exit of the PRB, the flow rate in the reactive filter is provided in eq. 24.

$$Q = q \cdot D = k_{filter} \cdot \frac{h_u - h_d}{L_{filter}} \cdot S_{filter} \tag{24}$$

where k_{filter} [m/s] represents the hydraulic conductivity of the filter, S_{filter} [m^2] and L_{filter} [m] respectively represent its cross-surface and length, h_u-h_d [m] represent the hydraulic head loss between the entrance and the exit of the filter, Q is the flow rate in the filtering gate [m^3/s], q is the flow rate per meter of depth of the aquifer [m^2/s], and D is the thickness of the aquifer [m].

Considering that $\phi = k_{soil} \cdot h + cste$ in the z-diagram, the combination of Eq. 21, 23 and Eq. 24 leads to the flow rate in a PRB (Eq. 25).

$$q = \frac{2 \cdot V_0 \cdot R \cdot \frac{k_{filter}}{k_{soil}}}{D \cdot \frac{L_{filter}}{S_{filter}} + \frac{1}{\pi} \cdot \frac{k_{filter}}{k_{soil}} \cdot ln\left(\frac{\sqrt{R^2 + R_d^2} - R}{\sqrt{R^2 + R_d^2} + R}\right)} \tag{25}$$

This equation represents the flow rate per meter of aquifer that can enter a filtering gate. For design purpose, the geometry of the filter (S_{filter} and L_{filter}), its hydraulic conductivity (k_{filter}), the radius of the drainage elements (R_d) and the width of cut-off walls (R) have to be selected according to the site conditions: q (minimum flow rate to be treated with respect to the width of the plume), V_0 (Darcy velocity of the groundwater on the site) and k_{soil} (permeability of the aquifer).

2.3 Residence Time as a Function of the Flow Rate

The first part of this paper was dedicated to the hydraulic aspect, which does not constitute the sole parameter for the design of a PRB. Indeed, the void volume of a filtering gate must be large enough to ensure a sufficient residence time. As a consequence, the design of a PRB must involve hydraulic and chemical considerations to prevent (a) any by-pass of the system, and (b) the break-through of the filter. The residence time T in a filter is deduced from the total flow rate Q and the porosity n of the reactive media, as mentioned in Eq. 26.

$$T = \frac{n \cdot S_{filter} \cdot L_{filter}}{Q} \tag{26}$$

Isovalues of residence time can thus be plotted in the (S_{filter}, L_{filter}) plane, as presented on Fig. 5 for the following parameters: V_0=40m/yr, R=80 m, n=0.4, R_d= 1.25 m, and k_{filter}/k_{soil} =10. All couples of

surface and length above a hyperbola generate a residence time greater than the corresponding isovalue and satisfy the chemical criterion. Fig. 5. Also contains a straight line corresponding to a specified flow rate q_s according to Eq. 25. All points under this line represent a higher flow rate than the specification (q_s). According to this figure, two conditions have to be satisfied simultaneously for the selection of a filter: (a) the residence time must be higher than the target, that is to say that the coordinates (S_{filter}, L_{filter}) must be above a selected hyperbola, and (b) the flow rate must be higher than q_s, that is to say that the coordinates (S_{filter}, L_{filter}) must be under the straight line. Combining the two previous conditions, a region of optimal geometry can be plotted as illustrated in grey on Fig. 5.

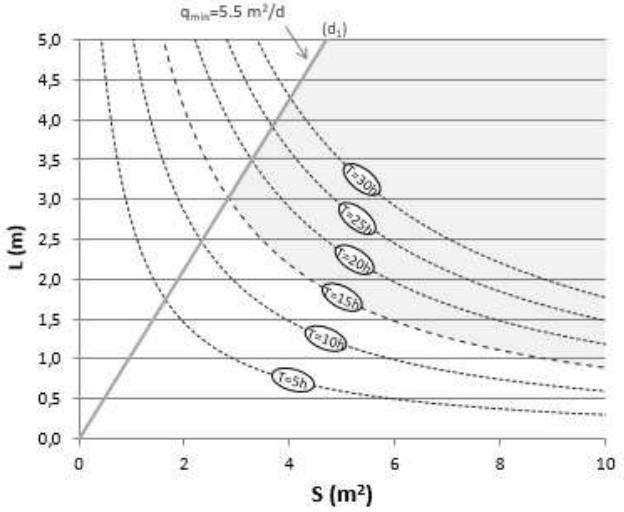

Fig. 5. Design guidance diagram.

4. Practical Application

Fig. 5 is a useful tool for the design of a PRB but it has to be redrawn when modifying the boundary conditions. To prevent this redrawing and to facilitate the design made by practitioners, Eq. 25 and 26 have been rewritten in terms of dimensionless variables.

$$\begin{cases} \frac{S}{D^2} = [A_1]^{1/2} \cdot \left[\frac{1}{A_2}\right]^{1/2} \cdot \left[\frac{1}{A_3} - \frac{1}{\pi} \cdot ln\left(\frac{\sqrt{1+A_4}-1}{\sqrt{1+A_4}+1}\right)\right]^{-1/2} \\ \frac{L}{D} = A \cdot \frac{D^2}{S} \end{cases} \quad (27)$$

where the dimensionless parameters are:

$$A_1 = \frac{q \cdot T}{n \cdot D^2} \qquad A_2 = \frac{k_{filter}}{k_{soil}} \qquad A_3 = \frac{2 \cdot V_0 \cdot R}{q} = \frac{Y_p}{R} \qquad A_4 = \frac{R_d}{R} \quad (28)$$

The system of Eq. 27 has been implemented in a guidance diagram provided on Fig. 6. This figure aims to design a PRB for all sets of boundary conditions and has to be used as follow:

i. Considering the width of the plume Y_p, select a cut-off wall length that meets $R \geq 2/\pi \cdot Y_p$,
ii. On Fig. 6.a, plot a vertical line at the corresponding $A_3 = Y_p/R$ and mark the intersection with the curve corresponding to the radius of the draining element ($A_4 = R_d/R$),
iii. Plot an horizontal line from this point and mark the intersection with the curve corresponding to the ratio $A_2 = k_{filter}/k_{soil}$ (See Fig. 6.b),
iv. Plot a vertical line from this point and note the value of α corresponding to the intersection with the abscissa. α represents the slope of the upper boundary of the optimal geometry region in the (S_{filter}, L_{filter}) plan (see Fig. 6.c).
v. Calculate the ratio $A_1 = q.T/n.D^2$ and select the corresponding hyperbola on Fig. 6.c. This hyperbola constitutes the lowest boundary of the optimal geometry region in the (S_{filter}, L_{filter}) plan.
vi. Select a filter section and length in the optimal region.

For illustration purposes, a practical application is proposed on Fig. 6. This application corresponds to the following boundary conditions: Y_p = 10 m, D = 3 m, q = 40 m^2/y, T = 120 h, k_{filter}/k_{soil} = 6 and n = 0.3. A length of 20 m has been chosen for the cut-off wall ($2R$). A higher value could be considered, but cut-off walls are expensive and practitioners try to minimize their length. A lower value could also be considered, but the safety factor decreases as R approaches $2/\pi \cdot Y_p$. Considering a typical draining trench with a radius of 1 m, the construction on the guidance diagram leads to an optimal region above the black bold lines on Fig.6.c. (α = 20 and A_1 = 0.2).

Finally, the design diagram demonstrates that a cut-off wall longer than *10* Y_p (i.e. Y_p /R > 0.*2*) significantly increases the hydraulic efficiency of the system. With this assumption, a ratio k_{filter}/k_{soil} higher than 10 prevents any hydraulic issue. Indeed, the optimal region becomes mainly influenced by the residence time (slope of the upper boundary higher than 100).

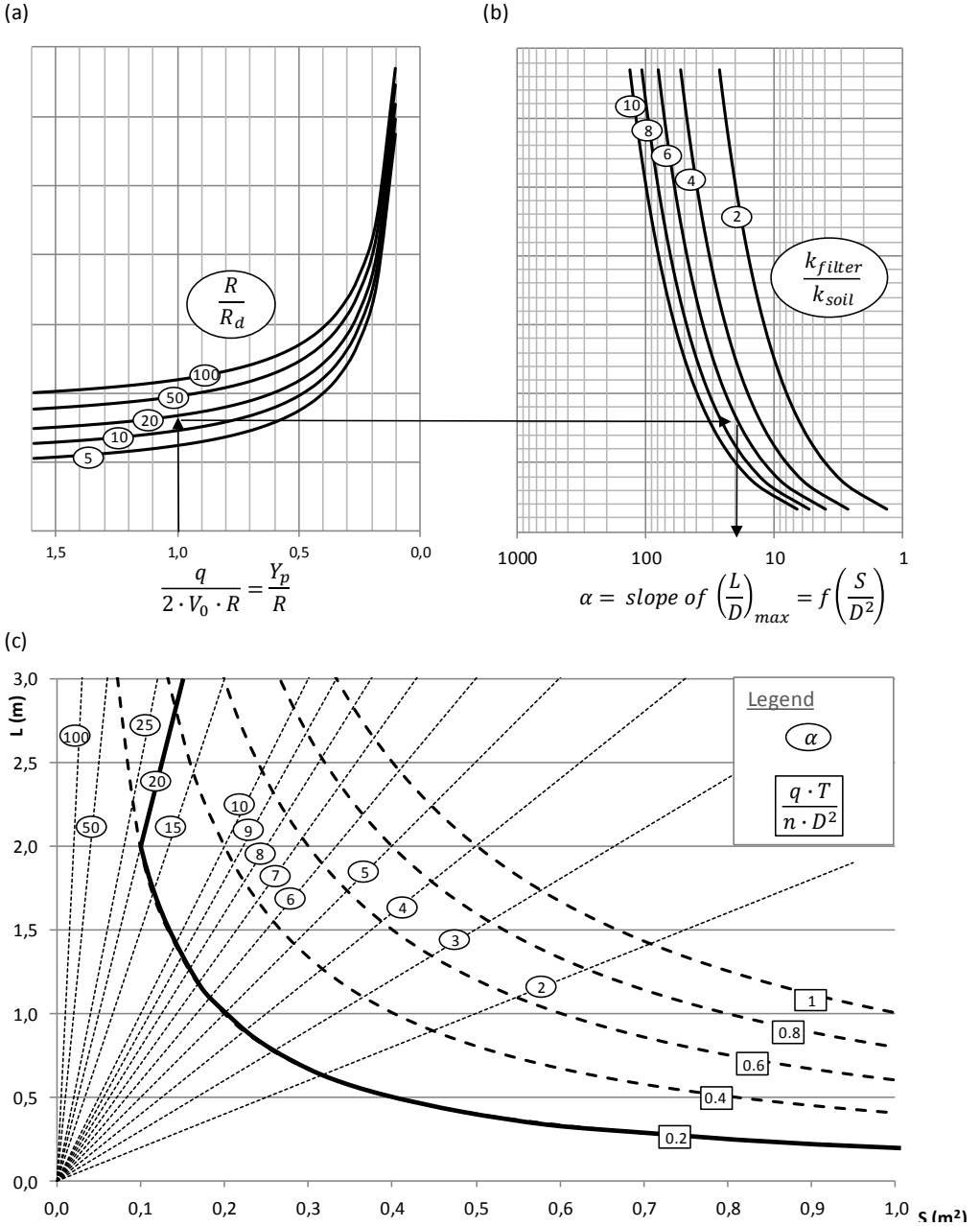

Fig. 6. Guidance diagram for the design of funnel-and-gate permeable reactive barriers.

5. Conclusion

Based on the Schwarz-Christoffel transformation, we developed an analytical solution of the flow rate in a PRB. This study demonstrated that the cut-off width has the most important impact on the capture zone and it leads to a design methodology for the reactive cell. According to this methodology, the section and length of a reactive cell are selected to ensure (a) a minimum flow rate, and (b) a minimum residence time in the porous media. The first condition is essential to capture the entire plume, while the second is mandatory to treat efficiently the contaminated groundwater. To meet these conditions, the design of a funnel-and-gate PRB comprises two steps: (a) a minimum cut-off width is selected to ensure a sufficient capture width, and (b) the filter's dimensions are selected on figure taking into account hydraulic and chemical constraints (residence time).

References

Blowes, D. W., C. J. Ptacek, et al. (1995). "Passive remediation of groundwater using in situ treatment curtains." *Geoenvironment 2000: Characterization, Containment, Remediation, and Performance in Environmental Geotechnics, Vols 1 and 2*(46): 1588-1607.

Chanson, H. (2009). *Applied Hydrodynamics: An introduction to ideal and real fluid flows*, CRC Press/Balkema.

Craig, J. R., A. J. Rabideau, Suribhatla, R. (2006). "Analytical expressions for the hydraulic design of continuous permeable reactive barriers." *Advances in Water Resources* 29(1): 99-111.

Gavaskar, A. R. (1999). "Design and construction techniques for permeable reactive barriers." *Journal of Hazardous Materials* 68(1-2): 41-71.

Guiger, N., J. Molson, et al. (1991). *Flonet v.1.02: Two-dimensional steady-state flownet generator*. Waterloo, Ontario, Waterloo Centre for Groundwater Research, University of Waterloo and Waterloo Hydrogeologic Software.

Klammler, H. and K. Hatfield (2008). "Analytical solutions for flow fields near continuous wall reactive barriers." *Journal of Contaminant Hydrology* 98(1-2): 1-14.

Klammler, H. and K. Hatfield (2009). "Analytical solutions for the flow fields near funnel-and-gate reactive barriers with hydraulic losses." *Water Resources Research* 45(2).

Klammler, H., K. Hatfield, et al. (2010). "Analytical Solutions for Flow Fields near Drain-and-Gate Reactive Barriers." *Ground Water* 48(3): 427-437.

Klammler, H., K. Hatfield, et al. (2010). *Capture flows of funnel-and-gate reactive barriers without gravel packs*, Algarve.

Liu, S., X. Li, et al. (2011). "Hydraulics Analysis for Groundwater Flow Through Permeable Reactive Barriers." *Environmental Modeling and Assessment* 16(6): 591-598.

McDonald, M. and A. Harbaugh (1988). *Techniques of Water-Resources Investigations Reports, A modular three-dimensional finite-difference ground-water flow model*, Book 6, Chap A1., US Geological survey.

McMurtry, D. C. and R. O. Elton (1985). "New approach to in-situ treatment of contaminated groundwaters." *Environmental Progress* 4(3): 168-170.

O'Hannesin, S. F. and R. W. Gillham (1998). "Long-term performance of an in situ "iron wall" for remediation of VOCs." *Ground Water* 36(1): 164-170.

Powell, R. M., D. W. Blowes, et al. (1998). *Permeable Reactive Barrier Technologies for Contaminant Remediation*. Washington.

Shoemaker, S., J. Greiner, et al. (1995). *"Permeable Reactive Barriers". Assessment of Barrier Containment Technologies: A Comprehensive Treatment for Environmental Remediation Application*. International Containment Technology Workshop, Baltimore, Maryland, Rumer, R. and Mitchell, J. Eds.

Streeter, V. L. (1948). *Fluid dynamics*, McGraw-Hill.

Warner, S. D., C. L. Yamane, et al. (1998). "Considerations for monitoring permeable ground-water treatment walls." *Journal of Environmental Engineering* 124(6): 524-529.

Warren, K. D., R. G. Arnold, et al. (1995). "Kinetics and mechanism of reductive dehalogenation of carbon tetrachloride using zero-valence metals." *Journal of Hazardous Materials* 41(2–3): 217-227.